



Research

Cite this article: Harvey TA, Bostwick KS, Marschner S. 2013 Directional reflectance and milli-scale feather morphology of the African Emerald Cuckoo, *Chrysococcyx cupreus*. J R Soc Interface 10: 20130391.
<http://dx.doi.org/10.1098/rsif.2013.0391>

Received: 29 April 2013

Accepted: 10 June 2013

Subject Areas:

biomaterials, biophysics, computational biology

Keywords:

feather, morphology, reflectance, directional reflectance, anisotropy, appearance

Author for correspondence:

Todd Alan Harvey
e-mail: todd.harvey@cornell.edu

[†]Present address: Department of Ecology and Evolutionary Biology, Yale University, PO Box 208015, New Haven, CT 06520, USA.

Directional reflectance and milli-scale feather morphology of the African Emerald Cuckoo, *Chrysococcyx cupreus*

Todd Alan Harvey^{1,†}, Kimberly S. Bostwick^{2,3} and Steve Marschner⁴

¹Department of Biomedical Sciences, ²Department of Ecology and Evolutionary Biology, ³Museum of Vertebrates, and ⁴Department of Computer Science, Cornell University, Ithaca, NY 14853, USA

Diverse plumages have evolved among birds through complex morphological modifications. We investigate how the interplay of light with surface and subsurface feather morphology determines the *direction* of light propagation, an understudied aspect of avian visual signalling. We hypothesize that milli-scale modifications of feathers produce anisotropic reflectance, the direction of which may be predicted by the orientation of the milli-scale structure. The subject of this study is the African Emerald Cuckoo, *Chrysococcyx cupreus*, noted for its shimmering green iridescent appearance. Using a spherical gantry, we measured the change in the directional reflectance across the feather surface and over a hemisphere of incident lighting directions. Using a microCT scanner, we also studied the morphology of the structural branches of the barb. We tracked the changes in the directional reflectance to the orientation of the structural branches as observed in the CT data. We conclude that (i) the far-field signal of the feather consists of multiple specular components, each associated with a different structural branch and (ii) the direction of each specular component is correlated to the orientation of the corresponding structure.

1. Introduction

Diverse plumages have evolved among birds through complex morphological modifications at multiple structural scales. Morphological differentiation between plumage patches allows for specialized signalling functions [1]. Pioneering work has recently affirmed the importance of direction to acoustical signalling in the context of avian mating [2,3]; similarly, direction is an essential aspect of visual signalling [4]. A bird's ability to control its plumage and reliably direct a visual signal towards a potential mate may also be critical to a male's reproductive success.

When investigating the link between morphology and specialized signal function, it is useful to subdivide plumage morphology into a hierarchy of structural scale, e.g. organism-, macro-, milli-, micro- and nano-scale. For example, plumage patches form at the organism-scale; feather vanes appear superficially flat at the macro-scale (greater than 1 mm); fibrous structures of the vane produces texture at the milli-scale (10 μm –1mm); surfaces and subsurfaces exhibit roughness at the micro-scale (less than 10 μm) and structural colour is produced by subsurface deposits at the nano-scale (on the order of the wavelength of light).

The complex interaction of light with the hierarchy of structural scale at and under the surface of the feather influences plumage appearance. Appearance can be discussed in terms of colour (hue, saturation and intensity defined physiologically [5–8] or perceptually [9]), direction (incident and viewing) [10] and location on the body of the organism. Avian research tends to focus on colour, treating appearance as directionally non-dimensional and limiting the investigation of variation across the surface of the organism to gross-scale colour patches [8,11].

Iridescence is a specialized directional signal produced by many species, including *C. cupreus* [12,13]. Through diffraction and interference [14], nano-scale



Figure 1. (a) *Chrysococcyx cupreus* male specimen in the Cornell Museum of Vertebrates. (b) The obverse face of a plucked tertial feather of the left wing.

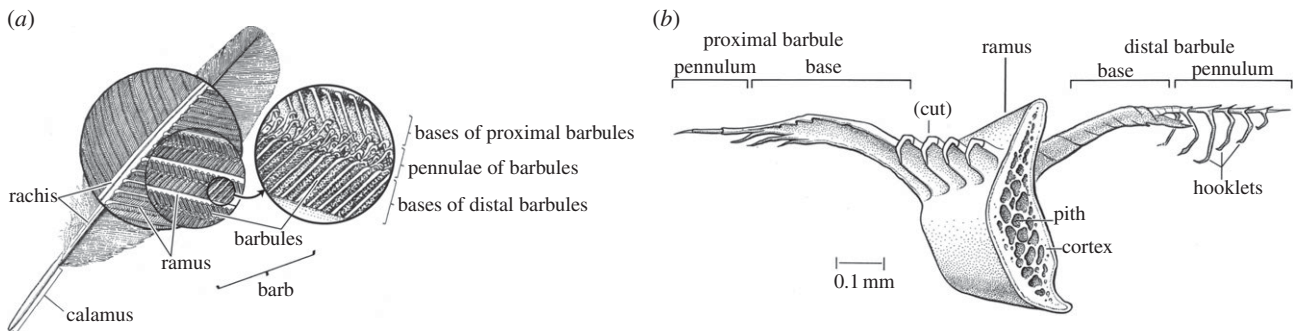


Figure 2. (a) The relationship between milli-scale barb structures and the macro-scale pennaceous feather vane. Adapted from [23]. (b) A cross-section of barb ramus with its attached distal and proximal barbules. Adapted from [24].

light-reflecting structures produce colours and patterns that shift and change as the bird, viewer or light moves, creating a dynamic appearance that draws the human—and presumably the avian—eye. To characterize this ephemeral signal, we measure reflectance from the plumage over a series of viewing and illumination directions [15,16]. A few researchers have sought to use such measurements when investigating the dependence between colour change and morphology of nano-scale structure [17–19]. In contrast, this paper is devoted to studying the dependence between the direction of the reflectance and the orientation of the milli-scale arrangements of nano-scale deposits within the barbs of the feather. We show how these embedded milli-scale structures, contouring the barb's surface, and unresolved with the unaided eye, play a critical role in directional signalling from plumage.

Plumage morphology varies with position on the body of the organism and real-world structures are rarely ideal Lambertian reflectors. Light therefore reflects differently at each position, even when incident and viewing directions remain constant. For example, during the courtship display of the male *Stellula calliope* hummingbird, the whiskered gorget feathers of the throat extend to form a localized planar region of purple iridescence [20]. The boundaries of the gorget are defined by spatial variation at the organism-scale; the spectra we perceive as purple is defined by spatial variation at the nano-scale. This paper will show that spatial variation at the milli-scale defines the *direction* of reflectance from plumage. Each scale defines a functionally different component of the appearance influencing the efficacy of the visual signal [21].

Given the many morphometric studies and the significant interest in bird coloration, surprisingly little investment has been placed in relating morphological modifications to variation in directional reflectance as a function of position on

plumage. We hypothesize that milli-scale structural modifications of feathers produce anisotropic reflectance, the direction of which may be predicted by the orientation of the milli-scale structure. In our investigation, the high-contrast shimmering plumage of *C. cupreus* (figure 1), coupled with its specialized barb morphology [22], offers an ideal study specimen to examine the correlation between spatial variation in milli-scale structure of the vane and directional variation in optical scattering. Our discoveries should assist in answering other, more behavioural inquiries, such as how critical is the female viewpoint to the success of male courtship displays?

2. Background

The pennaceous feather is constructed of two opposing vanes flanking the main shaft or rachis (figure 2a). Along the length of the rachis, barbs branch off at regular intervals. Each barb consists of a long thin shaft or ramus, from which branch two rows of barbules, one set proximally and the other distally. Each barbule consists of two main parts, a basal shaft and a more distal portion, the pennulum (figure 2b). The pennulae of distal barbules have series of hooklets that interlock the distal barbules of one ramus to the proximal barbules of the adjacent ramus. While not shown in the illustration, the modified pennulum of an iridescent barbule may manifest a broadened surface for reflecting light [25]. Although the typical feather vane superficially appears flat, its surface topography is in fact a three-dimensional, milli-scale network of specialized interconnected structures.

Nano-scale structures under the cortex or surface of feather barbs create one-, two- and three-dimensional spatial variation in the refractive index of the volume [25–29]. Light

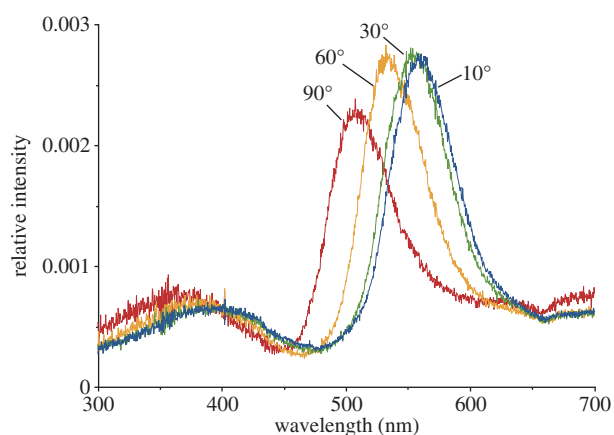


Figure 3. Normalized spectral reflectance of *C. cupreus* at 10°, 30°, 60°, 90° between incident and view directions. (Online version in colour.)

waves interact with these structures to produce a class of reflectance called structural colour [13]. One representation of structural colour, iridescence, changes colour based on the angle between illumination and viewing directions [30]. In *C. cupreus*, iridescence is produced by periodic layers of melanin sticks in the β -keratin of its barbs and barbules [12]; the single spectral peak in figure 3 is a product of constructive interference between waves reflected from the pairwise stack (up to 12) of keratin–melanin layers [22,31].

Durrer observed that the iridescence of *C. cupreus* is visible from an unusually large range of angles, not dissipating, as typical, from certain viewpoints [22]. He used electron microscopy to visualize the nano- and milli-scale structure of its feather and attributed its unusual iridescent behaviour to its modified feather morphology. His micrographs provided us the means to see its iridescence-producing, periodic layers of nano-scale melanin sticks that closely contour the milli-scale surface cortex of its barb. Additional modifications include the distal and proximal barbules—inclined up to 90° with respect to each other—capped by the cupped distal pennulae. Durrer described the impact of the distal barbule's pennulum geometry on colour production: its exposed convex shape not only supports the inclined distal and proximal barbules, but also reflects light in many directions.

Since Durrer's assertion of a relationship between geometric shape and the direction of reflected light, there have been many advances in other fields that have sought to clarify the behaviour of directional reflectance. The field of computer graphics has developed various mathematical models for geometric reflectance as a function of position and direction; efficiently and accurately capturing spatial and directional variation together is an active research area [32,33]. Considerable research has gone into explaining and predicting reflectance as a result of light interaction with variation in geometric form at various scales [34,35]. To address the geometric variation, whether random or regular, many models for isotropic [36] and anisotropic [37–40] surfaces have been developed.

All real-world materials exhibit variation in geometric form, which spreads reflected light in a range of directions commensurate to the degree of its variation and directional dependence. A 'glossy' material, having little micro-scale variation (i.e. roughness), concentrates reflected light in a small angular region near the direction of mirror reflection, also called the ideal specular direction (figure 4) [14]. Models based on the geometry of glossy specular reflection

from cylinders or rods have proved effective for a range of rough materials formed from milli-scale fibres, including hair [41,42], wood [43] and fabric [44,45]. Unlike the planar mirror, surfaces comprising fibres reflect light anisotropically, i.e. reflectance varies with rotation about the surface normal. Incident light from a single direction, striking the fibres, whose surfaces present a full circle of surface normals, reflects into a multitude of directions around the axis of the fibre (figure 5). Furthermore, each reflected direction forms an angle with the fibre axis equal and opposite to the incident direction (figure 6*a*). The set of all vectors at the same angle with a particular axis forms a cone centred on the axis.

These advanced models and methods have not been applied widely within the biological community. In this paper, we interpret plumage reflectance measurements in the context of what we understand about fibre surface reflection. We postulate that, like a fibre, a feather's ramus or barbule can be understood as an axis around which light reflects in a cone. Supporting our theory, a study of the iridescent neck plumage of *Columba livia* (Rock Dove) showed barbules reflecting light approximately perpendicular to their longitudinal axes [18]. Adapting existing surface reflectance theory to structurally coloured plumage necessitates the inclusion of light scattering events at subsurface interfaces. Thus, as the polished rod exhibits glossy surface reflectance commensurate with its degree of micro-scale *surface* roughness, so iridescent plumage exhibits glossy reflectance commensurate with its degree of micro-scale *surface and subsurface* roughness (figure 4). Accordingly, reflected light from a glossy ramus or barbule would be expected to form a thickened, blurry cone (figure 6*b*). The thickness of the cone depends on the roughness of the fibre; smooth fibres produce narrow, well-defined cones, whereas rough fibres produce broader ones.

In our study, directional dependence between incident and viewing direction is quantified using a gonireflectometer; it rotates the position of a light source and a detector around a study subject, enabling it to be illuminated and viewed from any direction. The incident and reflected angles are measured from the pole of the reflectance hemisphere, which coincides with the feather's surface normal. Measurements tabulated from directions on the hemisphere define the subject's bi-directional reflectance distribution function (BRDF) [10]. Light scattering adheres to the principle of reciprocity (which holds in the absence of nonlinear or magneto-optical effects that are not relevant for biological materials [46]): the result of a directional reflectance measurement is the same whether we hold the camera constant while moving the light over the hemisphere or vice versa [47,48].

A gonireflectometer can employ different detectors with varying capabilities. A photometer integrates all detected wavelengths in a single brightness measurement balanced to the human visual system. A spectrometer measures light across many spectral bands. Although classical photometers and spectrometers aggregate all detected light within their field of view, imaging detectors subdivide the field into individual cells on a grid, where each cell measures the reflectance of a substantially smaller area of surface than that of the full field of view [8,49]. A standard RGB colour camera is an example of a cost effective, high spatial resolution, low spectral resolution imaging detector [50]. It detects change in the reflectance from organisms, such as *C. cupreus*, which exhibit a dominant peak in the visible spectrum that shifts towards blue as a function of incident angle (figure 3). Most importantly, the RGB camera is entirely

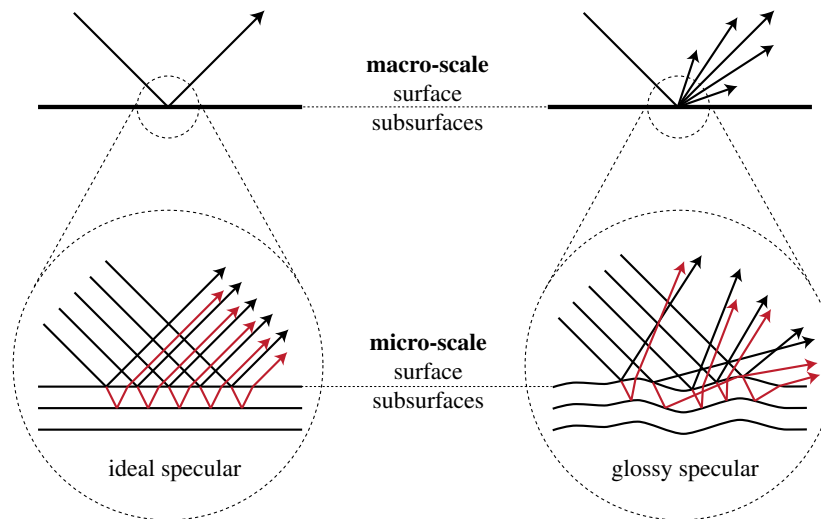


Figure 4. The variation in the direction of reflected light is commensurate to the variation in micro-scale roughness of structural interfaces at and under the surface. (Online version in colour.)

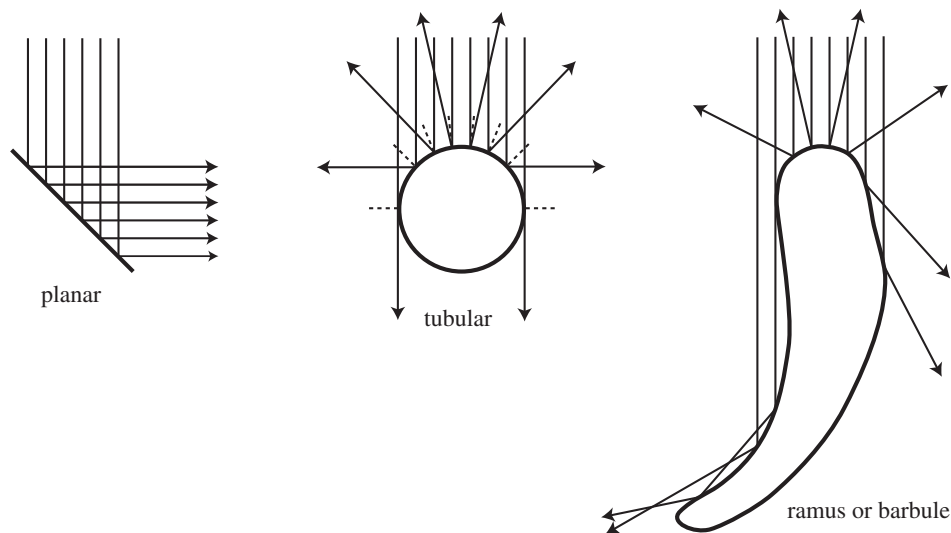


Figure 5. Collimated incident light reflects from a planar mirror in only one direction, but the mirrored rod reflects light in a circle of directions around its axis; likewise with the canonical ramus or barbule.

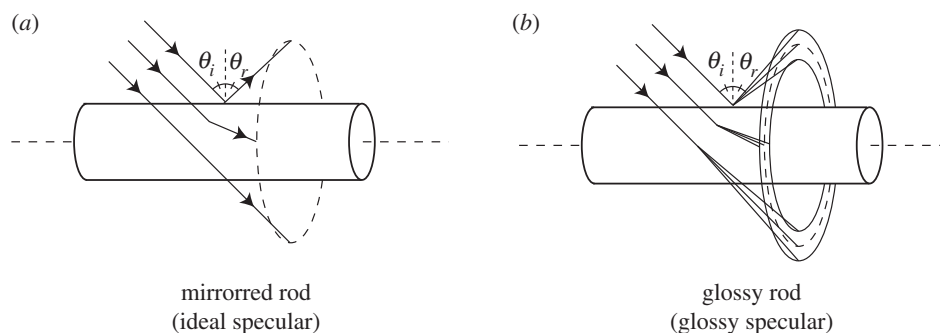


Figure 6. (a,b) Incident light from a single direction reflects into a cone of directions around the axis of a milli-scale elliptical fibre. Surface and subsurface roughness at the micro-scale thickens and blurs the reflection cone (figure 4).

sufficient when characterizing the spatial and directional variation of visible-spectrum iridescence, which is visible to both birds and humans.

The first well-known directional reflectance measurement of plumage employed a goniophotometer to detect luminous flux [51]. The researcher investigated the optical consequences of modified milli-scale hemispherical reflectors along the length of the iridescent barbules of the *Ptilinopus rivoli*

(White-bibbed Fruit Dove); hemispherical reflectors increased angular distribution of the directional reflectance, and thereby colour uniformity, when compared with species without the modification [51]. Since this study, the availability of low-cost fibre-optic spectrometers increased the application of goniospectrometers to survey the directional dependence of radiant flux from structurally coloured feathers [15]. Subsequent studies included measurements of

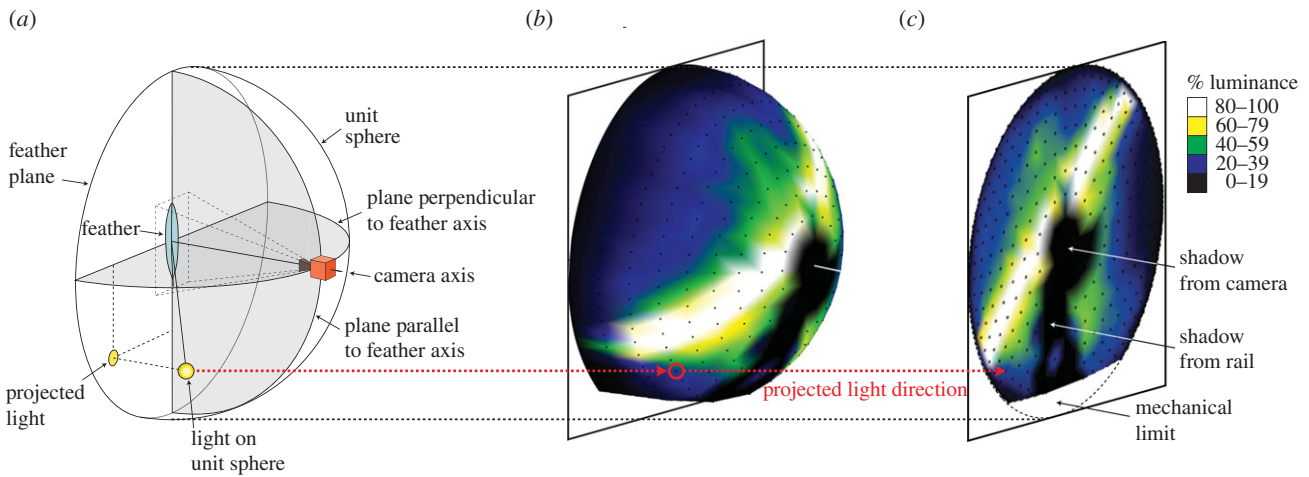


Figure 8. (a) Schematic of the spherical gantry configuration. (b) Luminance of the reflectance from a length of ramus sampled at 400 lighting directions over the hemisphere. (c) An orthographic projection of the reflectance hemisphere, or direction cosine plot. (Online version in colour.)

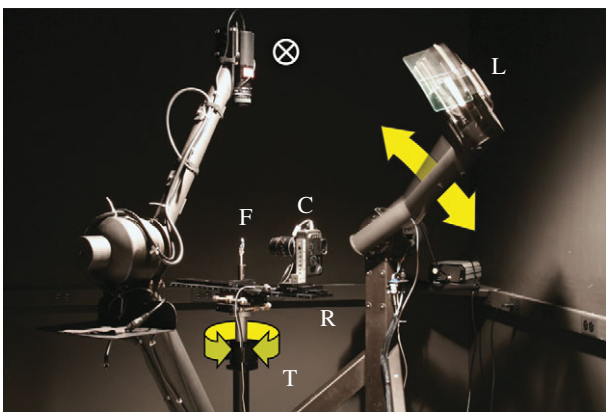


Figure 9. The camera (C) and feather (F) are affixed to a horizontal rail (R) atop a turntable (T). The feather may be illuminated from nearly any direction by light source (L). The second camera (⊗) was not used. Arrows represent axes of rotation. (Online version in colour.)

We measured the directional reflectance across the entire feather at high spatial and angular resolution. High spatial resolution resolved the milli-scale structure of the vane. High angular resolution resolved the glossy specular reflectance of the vane. We sampled the spatially varying light scattering over the entire surface of the feather by photographing it at 2 megapixel resolution ($78 \text{ pixels mm}^{-1}$) from a viewpoint normal to the obverse face of the feather, once for each of 737 illumination directions distributed uniformly over the sphere (figure 10). Approximately half (400) of the directions comprised the reflectance hemisphere. The remaining half, including the shared equator, comprised the transmittance hemisphere and will not be discussed further here.

The images of the feather acquired under different incident lighting directions were registered such that the same pixel in each image corresponded to the same location on the feather (figure 10). The light reflected from a single location on the feather was thus measured as a function of the direction from which it arrived by looking at the same pixel coordinate in each image. Directional reflectance was thereby tabulated pixel by pixel from the stack of registered images (for a complete review, see [16]). We used our data browsing software to select lines and rectangles on the feather surface and to compute average directional reflectance over the corresponding pixels. In this way, we visualized the directionally varying light scattering at any number of user defined, biologically relevant spatial positions and scales.

4.2. Reflectance metrics

Given these browsing tools, we assessed how the different biological structures contributed to the aggregate directional reflectance of the feather vane by measuring sets of pixels pertaining to the four biologically relevant, visible and resolved branches of the barb: ramus, base of the proximal barbule, base of the distal barbule and pennulum of the distal barbule (pennulae of proximal barbules are obscured by distal barbules) [16]. Because these structures repeat regularly along the vane of the feather, one interval is representative of the vane. We selected a line of pixels located on the ramus of one barb, then we moved our selection in a step-wise fashion at one-pixel intervals across the surface of the feather vane to reach the ramus of the adjacent barb (figure 11). We were able to identify incremental changes in directional scattering corresponding to the four structural elements of the barb. Next, we selected a large rectangular region of feather vane encompassing the entire progression and plotted the average directional reflectance to illustrate the relative contribution of each class of milli-scale structure to the far-field optical signature.

The first stage of analysis calculated the contribution of each of the four structures to the overall reflectance of the feather. Table 1 tabulates for each structure: (i) the *fractional image area* it occupies, (ii) the average reflectance of a cross-sectional unit area, integrated over the hemisphere (*directionally integrated reflectance*), (iii) the total reflectance of the entire structure, integrated over the hemisphere (*directionally and spatially integrated reflectance* = *fractional image area* × *directionally integrated reflectance*), and (iv) its *relative peak reflectance* in a single direction.

Since the camera and rail cast a shadow on the feather when illuminated from certain directions (figure 8), we had to fill in the missing reflectance measurements by interpolation. The interpolation was conducted by computing the convex hull of the directional reflectance. The volume of the convex hull is the integration of the reflectance over the hemisphere. In this manner, we computed the directionally integrated reflectance at each of 44 divisions between adjacent rami (figure 11). Finally, we proportionally assigned the directionally integrated reflectance at each division to the four structural branches of the barb in order to aggregate the reflectance per structural branch. We were not able to account for the reflectance outside the mechanical limit of the spherical gantry—fortunately, it does not figure prominently into the reflectance calculations of the medial vane.

The second stage of analysis addressed the orientation of the bands of high reflectance. As discussed in §3 and figure 7, reflections from fibres of the vane were postulated to produce cones, or sets of direction vectors at a fixed angle to the fibre axis. Since the intersection of such a cone with the direction hemisphere lies on

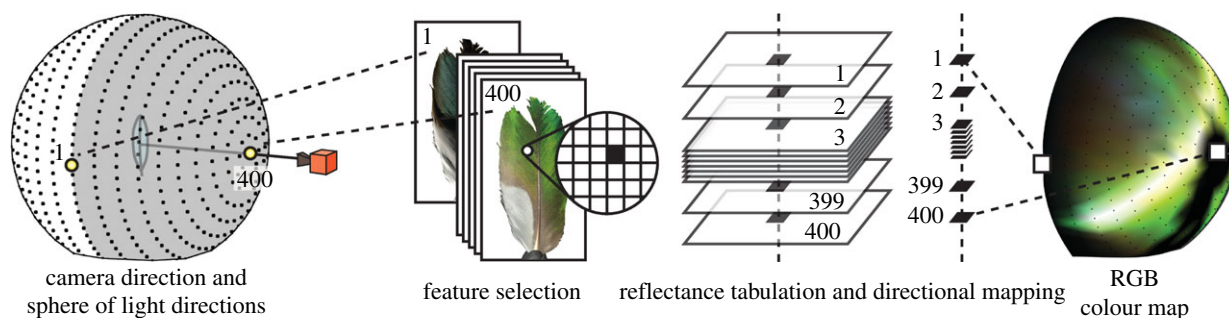


Figure 10. Each image of the feather was illuminated from a single direction on the uniformly sampled sphere. Since the camera direction was fixed, there exists a one-to-one correspondence between the pixels of the images and the structural features of the feather. The directional reflectance from any feature on the feather can be tabulated pixel-by-pixel from the registered images, where each image is illuminated from a different direction. For a given structural feature, the values of the tabulated reflectance were mapped to their corresponding directions on the reflectance hemisphere. (Online version in colour.)

a plane perpendicular to the fibre axis, we used plane fitting [43] to find the fibre axes consistent with the observed reflection cones. The inclination (ϕ) and azimuth (θ) of the reflectance of each structural branch is defined by the orientation of the normal vector of the plane (green plane in figure 7) fit to the reflectance distribution of each structure. This plane normal is expected to be the fibre direction. For each of the 44 divisions between adjacent rami in figure 11, we measured the inclination angle of the plane normal (similar to latitude) from the zenith of the reflectance hemisphere and the azimuth angle (similar to longitude) around the zenith in a direction counter-clockwise from the rachis. We assigned the measurements to their respective structural branches, and calculated the *average inclination*, *average azimuth* and the angular variance (*inclination variance* and *azimuth variance*) of each structure (table 1). These averages should predict the orientations of the respective structures. The weaker anisotropy of the reflectance of the distal pennulae proved more difficult to fit than other structures; two of the nine positions along its length required a manual estimation.

Lastly, in order to characterize which structural branches produce more or less sharply defined reflection cones, we measured the angular distribution of the anisotropic reflectance of each structural branch in a direction orthogonal to the fitted plane at *full width at half maximum* (FWHM).

4.3. MicroCT measurements and morphometrics

We used a microCT scanner (Xradia Versa XRM-500) to measure the longitudinal axis of the cortex of the barb, in order to approximate the longitudinal axes of the nano-scale melanin sticks underneath. We non-destructively measured a small region of the medial vane roughly equivalent in position to the region measured in figure 11. The scanner settings were 70 kilovolts, 6 watts, 85 microampere, $2.5 \mu\text{m voxel}^{-1}$ resolution, 8 s exposure time, 4000 projections.

Using the volume analysis software Osirix, first, we obliquely cross-sectioned the vane volume in planes parallel to the longitudinal axes of the bases of the proximal and distal barbules (figure 12a). From these oblique cross-sections of the vane, we measured the *average inclination* angle of the longitudinal axes of the bases of the barbules with respect to the macro-scale surface of the feather (table 1). Second, we viewed the vane in a direction normal to its macro-surface plane, and measured the *average azimuth* angle of the rami and bases of the barbules in a counter-clockwise direction with respect to the rachis.

5. Results

From the tabulated directional reflectance measurements of *C. cupreus*, we observed that different positions on the feather reflected light in different directions and with varying degrees

of anisotropy. In order to demonstrate how milli-scale morphology of the vane has impacted its optical signature, we correlated the orientation of each structural branch of the barb to the orientation of its directional reflectance. Figure 13 shows four representative signatures belonging to four milli-scale structures: ramus, base of the proximal barbule, base of the distal barbule and pennulum of the distal barbule. The morphology of these structures, their directional and integrated reflectance and their relative contribution to the reflectance of vane as a whole are organized below by subsection.

5.1. Barb axes predict the orientation of the reflectance cones

From microCT measurements, we observed the profile of the vane zigzagging in a plane orthogonal to the rami; the peaks of the profile repeated with a frequency equal to the interval of the rami branching from the rachis (a2–a3 of figure 12a). When we considered the construction in three dimensions, we found that the barbules, tilted up and away from the macro-surface of the vane, did not occupy the path of shortest distance (a perpendicular) from the rami to the peaked ridge-line. Instead, the barbules joined the rami to the ridgelines at acute complementary angles in the plane of the macro-surface (a1 of figure 12a and b1 of figure 12b). Therefore, we cross-sectioned the vane in planes normal to the macro-surface that contained the longitudinal axes of the base of the distal and proximal barbules (a4 and a5 reconstructed from the red and green planes in b3 of figure 12). From these two views, we measured the average angles at which the bases of the barbules, distal and proximal to the ramus, were tilted up and away from the macro-surface of the vane (ϕ_d and ϕ_p in figure 12). The topography of the vane is perhaps best described as forming a three-dimensional herringbone pattern where alternating rows of barbules are lifted up in opposite directions to form valleys with ridgelines capped by the distal pennulae (b2 of figure 12b).

We measured the whole hemisphere of directional reflectance at 44 discrete linear divisions across a one-barb interval between two adjacent rami of the medial vane. Following the description in §4.2, we generated 44 hemispherical maps shown as 44 circular plots in figure 11, one for each of the 44 divisions. Each of the structural branches of the barb was represented; we identified the location of the following structures from their reflectance signatures: ramus (plots 1–2), base of the distal barbule (plots 2–12), pennulum of the distal barbule (plots 10–14), base of the proximal barbule

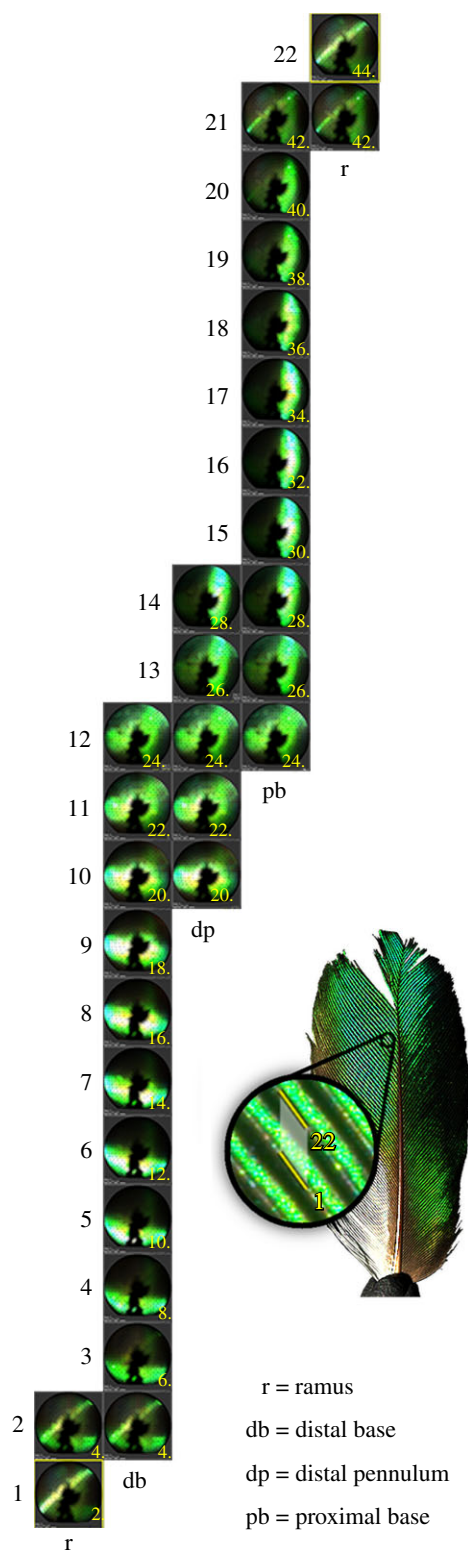


Figure 11. RGB directional reflectance of a region between two barbs of the medial vane was subdivided into 44 linear divisions, where each division measured 31 pixels \times 1 pixel (0.40 mm \times 13 μ m) and the vertical distance between the barbs is 0.56 mm. The average reflectance of 22 subsampled divisions is shown: (1) of line 1 along a length of ramus; (2–21) along sequential lines following step-wise movements; (22) of line 22 along a length of the adjacent ramus. (Online version in colour.)

(plots 12–21) and adjacent ramus (plots 21–22). Boundaries between structures produced sudden changes in directional distribution (plots 2 and 21), except where the distal pennulum bridged the orthogonally oriented reflectance of the bases of the distal and proximal barbules (plots 10–14).

The anisotropic reflectance of each structural branch (as identified in the 44 divisions) formed discrete bands on the hemisphere; however, the bands differed in width, position and sharpness. The base of the proximal barbule reflected incident light in a band roughly parallel to the proximodistal axis of the vane, but medially shifted from the surface normal. The base of the distal barbule reflected light in a band parallel to the mediolateral axis of the vane, but proximally shifted. Reflectance from the ramus crossed the axes of the vane in a proximal–lateral to distal–medial direction. We discovered that the ramus reflected light with the greatest degree of anisotropy, yielding the narrowest reflectance band on the hemisphere. The anisotropy of the reflectance from the bases of the proximal and distal barbules was weaker when compared with the ramus, so their reflectance bands are wider. The fourth structure we measured, the distal pennulum, manifested the weakest anisotropy. As a result of its structural function of bridging the two bases, the pennulum's directional reflectance changed dramatically over its length. Its inconsistent signal did not produce a signature readily recognized and fit to a singular cone.

The most important example of milli-scale structural orientation upon the directional reflectance of *C. cupreus* was manifested by the bases of the barbules and their respective bands of high reflectance inclined from the pole of the hemisphere by a factor of $2\times$ that of their structural inclination (b3 and b4 of figure 12*b*). In fact, the orientation of the bases of the barbules measured from the microCT reconstruction precisely predicted the orientation of the axes of the cones of reflectance fit from the directional reflectance measurements (table 1). The inclination equalled 10° or 11° and the relative azimuth between opposing bases equalled 89° ($\theta_r = 265^\circ - 176^\circ$ and $\theta_b = 266^\circ - 177^\circ$; see θ_r and θ_b in figure 12).

The width of the total reflectance of the entire base of the distal barbule is greater than that of the proximal barbule. The difference in the width can be traced in part to the $3\times$ greater variance in the inclination of the reflectance along the length of the base of the distal barbule (table 1). The greater variance effectively spreads the reflectance across a $2\times$ greater width of the hemisphere (21° when compared with 11° at FWHM) as seen in figure 14. We expect the increased variance is due to the apparent increased curvature along the length of the distal barbules, as seen in microCT reconstructions of the vane. Since no measurements were made, no predictions can be presented.

5.2. Directionally and spatially integrated reflectance of discrete structures

Measurements of directionally and spatially integrated reflectance as a function of the barb's branching milli-scale structure makes it possible to compare the relative contributions of each branch to the reflectance of the vane (table 1).

5.2.1. Base of the proximal and distal barbules

Arrays of parallel barbule bases adjoined to form two contiguous, reflective, milli-scale surfaces proximal and distal to the ramus. In aggregate, the surface of the bases of the barbules comprised 77 per cent of the projected surface area of the obverse face of the vane. In addition to their surface area advantage, their average directionally integrated reflectance was $19\times$

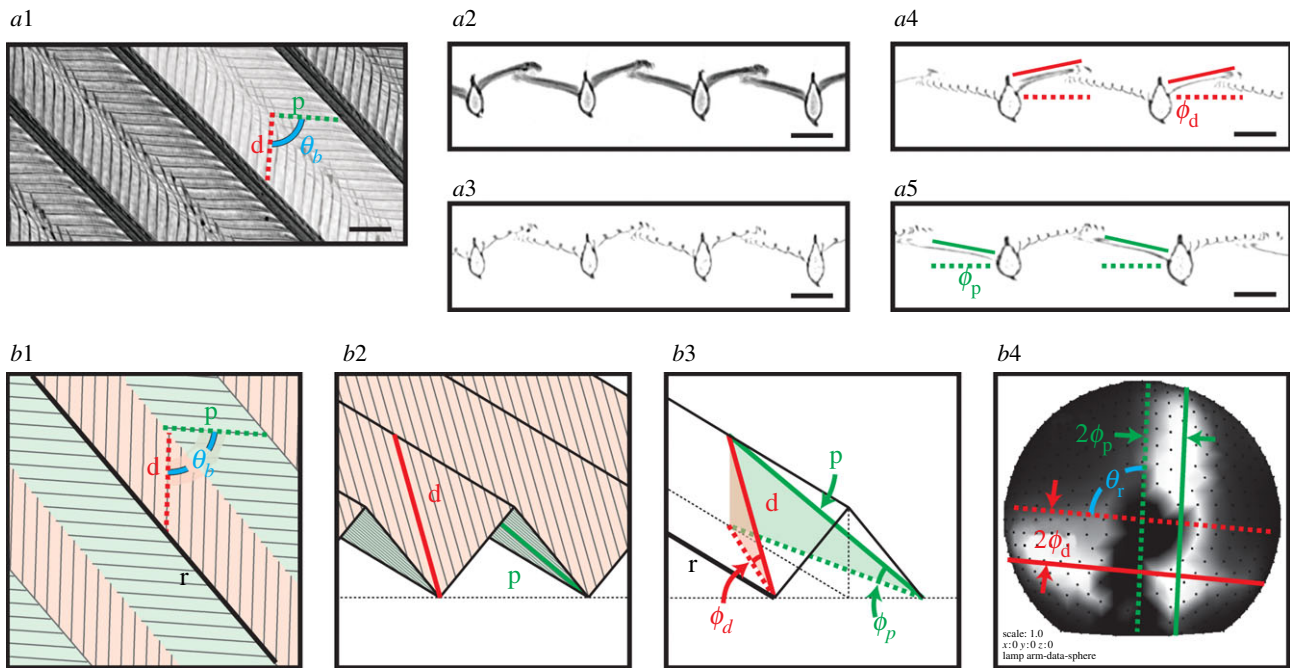


Figure 12. MicroCT images (*a*) and schematic diagrams (*b*) of the barb structure of the medial vane. (*r*) Ramus. (*d*) Distal barbule. (*p*) Proximal barbule. (ϕ_d) Inclination angle of the base of the distal barbule. (ϕ_p) Inclination angle of the base of the proximal barbule. (θ_b) Azimuth angle between bases of the distal and proximal barbules projected in the plane of the macro-surface. (θ_r) Angle between the two planes fitted to the reflectance of the bases of the distal and proximal barbules. (*a*) MicroCT reconstructions: (a1) Obverse view oriented with rachis up and macro-surface in the plane of the page matches the gantry experimental setup. (a2a3) Transverse cross sections of the rami. (a4) Longitudinal cross-sections of the base of the distal barbule in plane with the macro-surface normal. (a5) Longitudinal cross-sections of the base of the proximal barbule in plane with the macro-surface normal. A slab consists of multiple slices. Scale bar, 100 μm . (*b*) Schematic diagrams: (b1) Obverse view. (b2) Oblique transverse cross-section. (b3) Inclination of the bases of the distal and proximal barbules. (b3) Average directional reflectance of a rectangle region containing distal and proximal barbules. (Online version in colour.)

Table 1. Reflectance and morphology statistics of four structural branches of the barb. Reflectance is calculated from a view direction roughly normal to the obverse face of the feather. Morphology is reconstructed from microCT where the rami define the local macro-surface plane.

reflectance	ramus	distal base	distal pennulum	proximal base
fractional image area ^a	0.09	0.35	0.14	0.42
directionally integrated reflectance ^a	0.01	0.46	0.04	0.49
directionally and spatially integrated reflectance ^a	0.00	0.44	0.02	0.54
peak reflectance ^b	0.15	0.73	0.32	1.00
average inclination (deg)	8	11	10	10
inclination variance (deg)	1	15	21	5
average azimuth (deg)	40	176	35	265
azimuth variance (deg)	1	11	88	12
full width at half maximum (deg)	—	21	—	11
morphology				
average inclination (deg)	0	11	—	11
average azimuth (deg)	41	177	—	266

^aRelative to the sum total.

^bRelative to maximum component.

greater than that of the rami and distal pennulae combined. The directionally and spatially integrated reflectance of the bases of the distal and proximal barbules, 44% and 54%, respectively, are proportionally equivalent to their individual projected surface areas. In sum, they produce 98% of the reflectance of the vane. No other branch of the barb produces comparable reflectance.

5.2.2. Pennulum of the distal barbule

The convex curvature of the pennulum distributed reflectance over the greatest portion of the hemisphere; as such, the pennulum produced the weakest anisotropy of the four structural branches of the barb, effectively minimizing the reflectance in any given direction. But anisotropy is not the only factor working to minimize the intensity of the reflectance of the

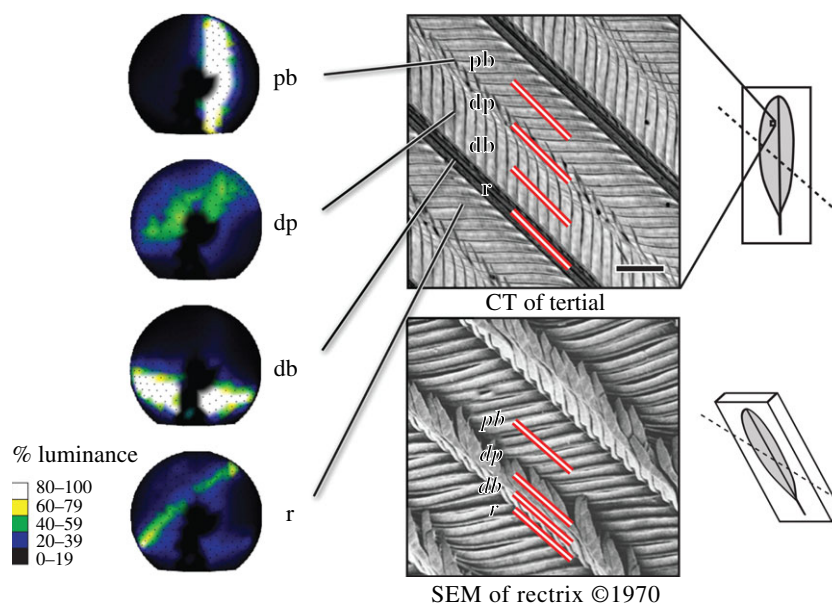


Figure 13. The luminance of the directional reflectance of different components of the barb—ramus (*r*), base of the distal barbule (*db*), pennulum of the distal barbule (*dp*), base of the proximal barbule (*pb*)—was measured from a direction normal to the macro-surface of the medial vane of a tertial feather and plotted in direction cosine space. The three-dimensionality of the vane's milli-scale structure is not readily apparent in the microCT image reconstructed from a viewpoint perpendicular to the vane's macro-surface. By comparison, Durrer's SEM displays a rectrix feather rotated around the axis of its rami, such that the bases of the proximal barbules lie in proximity to the plane of the image, while the bases of the distal barbules rise up out of the plane of the image and are foreshortened. The lines (*r*, *db*, *dp*, *pb*) on the vane are not drawn to scale, but represent the approximate linear divisions (1, 6, 12, 16) shown in figure 11. MicroCT scale bar, 100 μm . SEM adapted from Durrer & Villiger [22], Springer Berlin/Heidelberg. Reproduced with kind permission from Springer Science and Business Media. (Online version in colour.)

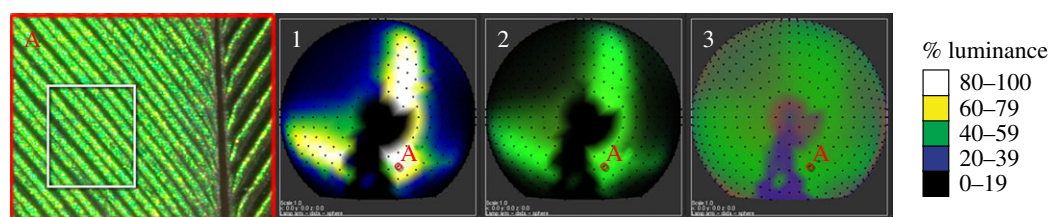


Figure 14. Image A contains a feather photographed from the direction normal to its surface and illuminated from the direction circled in red (and labelled A) in plots 1, 2, 3. The average directional reflectance of the rectangular region of image A ($1.4 \times 1.7 \text{ mm}$) containing rami, distal and proximal barbules of the medial vane is plotted in colour maps: (1) luminance, (2) RGB and (3) chromaticity.

pennulum. The average directionally integrated reflectance of the pennulum was only 9% of that of either barbule base. Its relatively low average directionally integrated reflectance is further compounded by its relatively small projected surface area (14%), yielding an exceptionally low (2%) directionally and spatially integrated reflectance when compared with that of the bases of the barbules (98%).

5.2.3. Ramus

Of all the structural branches, the ramus reflects most anisotropically, concentrating reflectance within the narrowest cone. Since high anisotropy concentrates reflected energy in the narrowest range of directions, the potential for exceptionally high reflectance exists. Yet, the ramus measured relatively low reflectivity; its peak reflectance was least of all branches of the barb (15% of the base of the proximal barbule). The narrow width of its reflectance band compounded by its low reflectivity yielded a diminutive average directionally integrated reflectance of 1%. Finally, its exceptionally low-projected surface area (9%) further reduced its directionally and spatially integrated reflectance to a negligible quantity, virtually eliminating its contribution to the overall feather appearance in the far-field.

5.3. Emergent properties of the vane in the far-field

Section 5.2.3 presented results of directionally and spatially integrated reflectance as a function of the barb's branching structure. In this section, we combine the reflectance of the individual structural branches of the barb to investigate the emergent properties of the feather. First, we present the far-field optical signature of the feather, i.e. the directional reflectance of a small region of the feather approximating the resolution limit of the human eye at a distance where the individual milli-scale structures of the feather cannot be resolved. Then, we address the shift and symmetry in the reflectance induced by the macro-scale distortions of the two feather vanes.

We selected a rectangular region of the medial vane containing several barbules (A of figure 14) and plotted the average directional reflectance of this region (1–3 of figure 14). The two bands of high reflectance from the barbule bases dominated the far-field optical signature. The low reflectance of the distal pennulae, the influence of which is seen in the chromaticity plot, hardly registered in the luminance and RGB plots. Reflectance from the rami is not detectable in any of the plots. From this measurement, we see that the far-field optical signature of a small rectangular region of the feather vane is

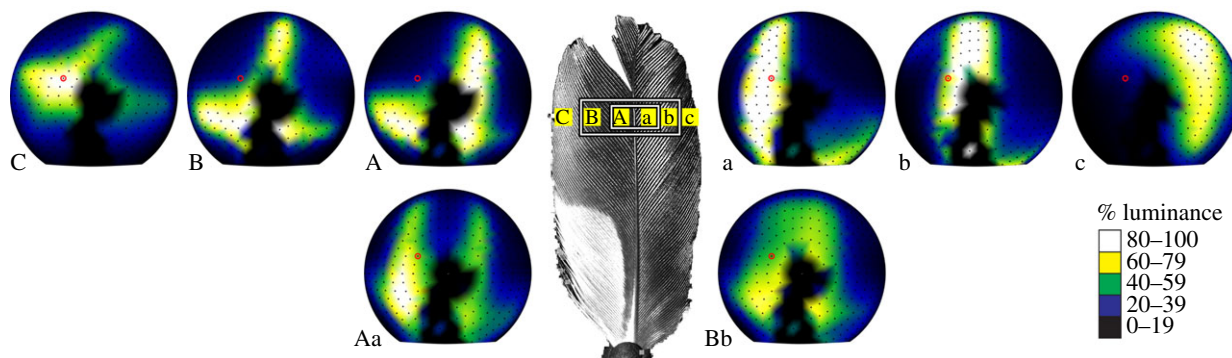


Figure 15. Average directional reflectance of rectangular regions of *C. cupreus*: (A–C) three regions of the medial vane, (a–c) three regions of the lateral vane, and (Aa and Bb) two regions spanning both vanes. Luminance plotted in direction cosine space. The circled directions (red in the colour figure) denote the direction of the light illuminating the feather in the image. (Online version in colour.)

explained by a subset of the milli-scale geometry of that region, which the eye cannot resolve, the bases of the barbule; the remaining milli-scale structures are irrelevant.

Yet, the influence of another and larger structural scale—the macro-scale—becomes apparent in the far-field when the feather is viewed as a whole. To ascertain the influence of the macro-scale structure (e.g. curl and twist of the vane) upon the crossed reflectance bands produced by the milli-scale structure, we subdivided the feather and measured the far-field optical signature at each subdivision (figure 15). At six sample sites (A–C and a–c), we measured a significant mediolateral shift in the reflectance of the base of the proximal barbule. For regions near the central shaft, such as sites (A, a), the vane opposite the light source reflected in the polar direction. For regions near the marginal edge, such as sites (C, c), the vane in the direction of the light source reflected in the polar direction. Whether measured in proximity to its central shaft or its marginal edge, the reflectance exhibited symmetry between the two vanes.

Owing to the symmetry of the milli-scale structure of the opposing vanes, the reflectance from a region comprising equal portions of both vanes (Aa of figure 15) contained two opposing bands in the proximodistal axis of the vane and double the reflectance in the mediolateral axis. In the broader region (Bb), the two opposing bands shifted medially, merging as a single blurry band straddling the polar direction.

In summary, iridescence was viewed in more directions than otherwise possible due to the symmetry of the inclined bases of the barbules of the two feather vanes. A feather that reflects light from just one structure can cover only one band on the hemisphere. The *C. cupreus* feather expands its coverage over the hemisphere through its four bands originating from four structures belonging to two vanes. The two bands of a single vane are complemented by the two bands of the opposing vane to cover a greater portion of the reflectance hemisphere when compared with one vane alone. At near distance, the symmetry of the multiple bands produce rings and eyelets. At far distance, they increase the blur, directional distribution and isotropy of its signal.

5.4. Grazing angle reflectance of the rami

On the whole, the directionally and spatially integrated reflectance of the ramus was negligible (§5.2). Yet, some components of its reflectance actually augmented the dominant far-field optical signature of the feather. Unlike the bases of the barbules, the reflected light around the axis of

the ramus was largely biased in directions approaching the plane of the macro-surface (figure 16). In directions A and C of plot 1, we observed that grazing incident illumination produced increased reflectance (at least $2.5\times$ greater) in the direction of the macro-surface normal. In plots 2 and 3, we observed that the reflectance of the rami, like that of the bases of the barbule, was both brilliant and saturated green. Since the ramus was oriented 45° from that of the barbule bases, it had the potential to produce a signature distinguished from that of the bases. On the contrary, we found that the same grazing incident illumination that produced a brilliant green ramus, also produced brilliant green barbule bases. At high magnification, we resolved the ramus independently of the adjoining fields of green of either barbule base. But without magnification, the undifferentiated signal of the ramus was subsumed by that of the barbule bases. The ramus effectively contributed an additional 9% fractional surface area to the signal of the barbule bases (35% and 42%) when illuminated from certain grazing angles.

6. Discussion

The feather vane is constructed upon a hierarchy of morphological scale (including nano-, micro-, milli- and macro-scales), for which we found corresponding optical consequences. Our results supported our hypothesis that the direction of reflectance from a feather can be explained by the orientation of its milli-scale structure. We developed a geometrical model that accurately predicted the direction of a feather's reflectance from its component parts.

Previous research has explained how colour is produced from the interference of light waves with periodic nano-scale structure under the cortex of the barbs of *C. cupreus* [22]. Rather than focus on the wavelength or colour of the reflectance, we sought to study the direction of the reflectance in relation to the direction of the nano-scale structure of the barbs of the vane. When measuring morphology and reflectance by traditional methods, rami and barbules must be dissected from the composite vane [18,19,49,52]. The required dissections and cross-sections make it practically impossible to reconstruct the direction of the longitudinal axes of the nano-scale sticks responsible for light reflectance from various branches of the barb. We observed the layers of nano-scale sticks contouring the milli-scale barb cortex in Durrer's electron micrographs. Since the milli-scale barb cortex can be readily imaged by microCT, we developed a

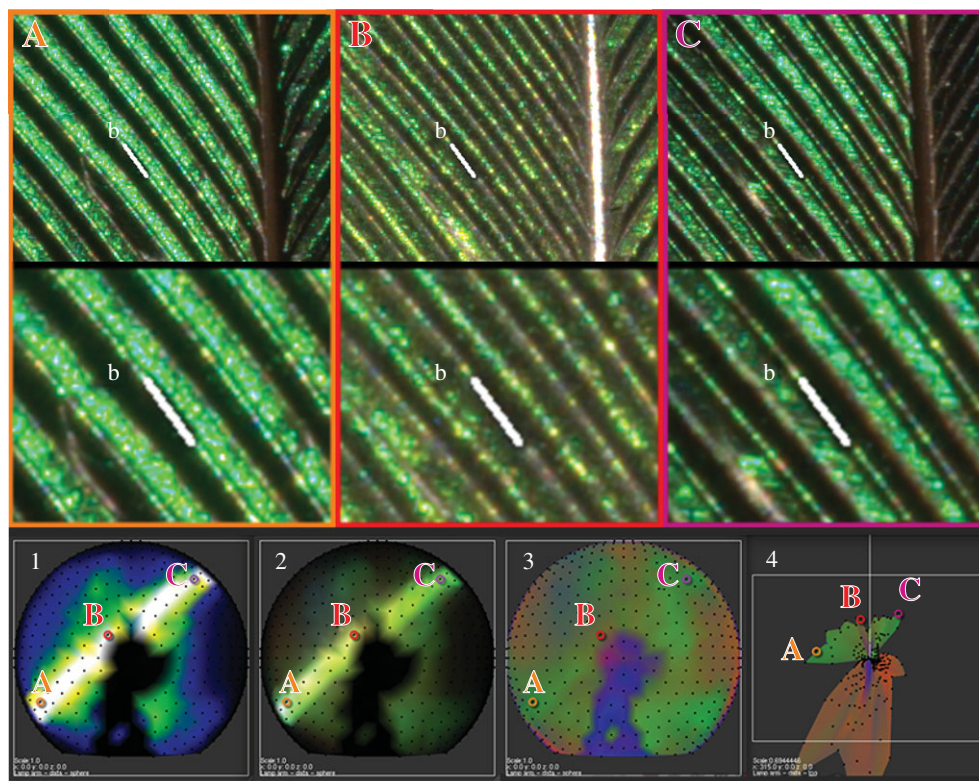


Figure 16. (A–C) *Chrysococyx cupreus* illuminated from different directions and imaged at two magnification scales: (A) illuminated from a proximal–lateral direction with respect to the feather vane. (B) illuminated near normal incidence. (C) illuminated from a distal–medial direction with respect to the feather vane. (1–4) The average directional light scattering of the linear region of barb ramus b ($0.40\text{ mm} \times 13\text{ }\mu\text{m}$) is plotted in four formats: (1) luminance, (2) RGB, (3) chromaticity and (4) chromaticity colour map on a three-dimensional spherical plot, where the radii of each direction on the unit sphere are scaled by their respective luminance values.

novel method using the cortex as a proxy for the sticks. Using a microCT scanner to measure morphology and an imaging scatterometer (spherical gantry) to measure reflectance, we correlated the direction of the proxy geometry to the direction of the reflectance from the nano-scale structures of the vane.

Our protocol was non-destructive and, equally importantly, preserved the morphological relationships within the fabric of the intact vane. By comprehensively measuring the entire feather and eliminating dissection, our approach provided tremendous flexibility during post-acquisition investigations, when we digitally isolated the component parts of the feather to study the morphology and reflectance of each part, separately and in aggregate. We investigated not only the individual reflectance signatures of the component parts at the milli-scale, but also the spatially integrated reflectance of the component parts at the macro-scale as seen in the far-field. While measurements of the intact vane were critical to identifying the spatially integrated signal seen by other organisms, only when milli-scale structures were analysed in the context of the intact vane could we identify the component parts most relevant to its integrated signal.

Our geometrical model correctly predicted the integrated signal of the structural innovations of *C. cupreus*, the three-dimensional herringbone zigzag of milli-scale structure formed by the inclined bases of its barbules. Unlike the extended distal barbules of many glossy iridescent feathers, those belonging to the wing, tail and body of *C. cupreus* did not extend so far as to cover the proximal barbules and rami. The signal from these exposed bases of the proximal barbules proved as relevant as those of the distal barbules. The inclined orientation of adjacent bases of a single vane produced a two-part signal

(comprised two orthogonal bands of high reflectance which cross at a position on the hemisphere shifted from the macro-surface normal) with minimized overlap and maximized directional distribution over the hemisphere. The bilateral or mirrored symmetry of the two-vaaned signal maximized coverage in three of four quadrants of the reflectance hemisphere, with twice the reflectance in the proximal direction. Though we measured one feather, all the feathers of *C. cupreus* grow in the same direction (towards the tail) wrapped around the proximal–distal axis of the organism (figure 1). So when one feather has twice the reflectance in a proximal (face-forward) direction, all the feathers have twice the reflectance in a face-forward direction.

Although iridescence was viewed in more directions than otherwise possible, for a given location on an individual feather, a large fraction of hemisphere remained untouched. Because we can relate the feather's reflectance at the milli-scale to that at the macro-scale, we can explain how some iridescent green reflectance emerges from all the feathers over *C. cupreus*' body (figure 1), regardless of their orientation. Our measurements in §5.3 demonstrated how the smoothly contoured macro-scale shape of the feather shifted the directional distribution of reflected light to increase coverage over the hemisphere. At near distance (A, B, C, a, b, c of figure 15), sharp specular rings outline individual feathers. At far distance (Bb of figure 15), the integrated signal was blurred and iridescent green colour was viewed over a greater range of directions with increased isotropy. Our results justify Durrer & Villiger's [22] observation that iridescence from *C. cupreus* can be viewed from many more directions than typical avian iridescent plumage.

We also confirmed Durrer and Villiger's claim that morphological adaptations extend iridescent colour production

from the base to the pennulum of the barbule, but contrary to their writings we demonstrate that the increased angular reflectance is *not* due to colour production from the distal pennulae. Despite its iridescent colour, surface area and unobstructed position at the peak, the distal pennulae does *not* significantly contribute to the reflectance of the feather. We assert that the primary role of the distal pennulum is structural. The pennulum is a fascinating, anomalous structure that connects the bases of opposing barbules, forming the peak of the zigzag of the vane. The distal pennulum probably developed a broad cross-section primarily to capture the tip of the proximal barbule to support the colour production of the bases of the distal and proximal barbules, rather than function as reflectors themselves.

Our predictive model explains the signalling potential of *C. cupreus* and enables discussion about the link between function and morphology that leads to adaptive innovations in the individual component parts of its feathers. Where some birds employ colour and plumage patches to create discontinuities and contrast, *C. cupreus* makes maximum use of the directional constraints of anisotropic glossy specular reflectance to create eye-catching patterns of high and low reflectance. Rather than displaying dramatic colour change, *C. cupreus* shimmers idiosyncratically when incident light and view directions vary. The courtship behaviour of *C.*

cupreus is undocumented, and it is unknown if the ringing pattern, easily observed when viewing the organism in directions perpendicular to its proximal–distal axis (figure 1a), is sexually selected. Less obvious, but perhaps more influential, milli-scale structures bias signals in face-forward directions, rim-lighting the contours of the body. Might the readily observed ringing be a byproduct of selective pressure to tilt the distal barbules, facilitating communication along the bird's proximal–distal axis? Our directional scattering studies have an important future in complementing fieldwork to answer questions like these in avian signalling.

Acknowledgements. Thanks to Dr Ellis Loew, Dr John Hermanson and Dr Susan Suarez, Cornell University; Dr James Harvey, CREOL, University of Central Florida; and Dr Richard Prum, Yale University for their guidance and review of this manuscript; Kalliope Stouraras, University Freiburg, for her translation of the Durrer and Villiger manuscript; Josh VanHouten, Yale University, and Mark Riccio, Cornell University, for microCT measurements; and Dr Donald Greenberg, Dr Jon Moon, Dr Jaroslav Křivánek, Wenzel Jakob, Edgar Velázquez-Armendáriz and Hurf Sheldon, Cornell University, for their contributions in Computer Graphics.

Data availability. Data deposited in the Dryad Repository: (doi:10.5061/dryad.332b5)

Funding statement. This research was supported by funding from the National Science Foundation (NSF CAREER award CCF-0347303 and NSF grant CCF-0541105).

References

- Hill GE, McGraw KJ. (eds) 2006 *Bird coloration, vol. 2: function and evolution*. Cambridge, MA: Harvard University Press.
- Patricelli GL, Dantzker MS, Bradbury JW. 2007 Differences in acoustic directionality among vocalizations of the male red-winged blackbird (*Agelaius phoeniceus*) are related to function in communication. *Behav. Ecol. Sociobiol.* **61**, 1099–1110. (doi:10.1007/s00265-006-0343-5)
- Patricelli GL, Dantzker MS, Bradbury JW. 2008 Acoustic directionality of red-winged blackbird (*Agelaius phoeniceus*) song relates to amplitude and singing behaviours. *Anim. Behav.* **76**, 1389–1401. (doi:10.1016/j.anbehav.2008.07.005)
- Lythgoe JN. 1979 *The ecology of vision*. New York, NY: Oxford University Press.
- Goldsmith TH. 1990 Optimization, constraint, and history in the evolution of eyes. *Q. Rev. Biol.* **65**, 281–322. (doi:10.1086/416840)
- Endler JA, Mielke PW. 2005 Comparing entire colour patterns as birds see them. *Biol. J. Linn. Soc.* **86**, 405–431. (doi:10.1111/j.1095-8312.2005.00540.x)
- Stoddard MC, Prum RO. 2008 Evolution of avian plumage color in a tetrahedral color space: a phylogenetic analysis of new world buntings. *Am. Nat.* **171**, 755–776. (doi:10.1086/587526)
- Kim MH *et al.* 2012 3D imaging spectroscopy for measuring hyperspectral patterns on solid objects. *ACM Trans. Graphics (TOG)* **31**, 38. (doi:10.1145/2185520.2185534)
- Wyszecki G, Stiles WS. 2000 *Color science: concepts and methods, quantitative data, and formulae*. Wiley classics library. New York, NY: John Wiley & Sons.
- Nicodemus F, Richmond J, Hsia J, Ginsberg I, Limperis T. 1977 *Geometric considerations and nomenclature for reflectance*. Washington, DC: National Bureau of Standards, US Department of Commerce.
- Stoddard MC, Prum RO. 2011 How colorful are birds? Evolution of the avian plumage color gamut. *Behav. Ecol.* **22**, 1042–1052. (doi:10.1093/beheco/arr088)
- Durrer H. 1977 Schillerfarben der Vogelfeder als Evolutionsproblem. *Denkschriften der Schweizerischen Naturforschenden Gesellschaft* **91**, 1–127.
- Prum RO. 2006 Anatomy, physics, and evolution of structural colors. In *Bird coloration, vol. 1: mechanisms and measurements* (eds GE Hill, KJ McGraw), pp. 295–353. Cambridge, MA: Harvard University Press.
- Hecht E. 1998 *Optics*. Boston, MA: Addison Wesley.
- Osorio D, Ham A. 2002 Spectral reflectance and directional properties of structural coloration in bird plumage. *J. Exp. Biol.* **205**, 2017–2027.
- Harvey TA, Bostwick KS, Marschner SR. 2013 Measuring spatially- and directionally-varying light scattering from biological material. *J. Visualized Exp. JoVE* **75**, e50254. (doi:10.3791/50254)
- Doucet SM, Shawkey MD, Hill GE, Montgomerie R. 2006 Iridescent plumage in satin bowerbirds: structure, mechanisms and nanostructural predictors of individual variation in colour. *J. Exp. Biol.* **209**, 380–390. (doi:10.1242/jeb.01988)
- Nakamura E, Yoshioka S, Kinoshita S. 2008 Structural color of rock dove's neck feather. *J. Phys. Soc. Jpn* **77**, 124801. (doi:10.1143/JPSJ.77.124801)
- Stavenga DG, Leertouwer H, Marshall NJ, Osorio D. 2010 Dramatic colour changes in a bird of paradise caused by uniquely structured breast feather barbules. *Proc. R. Soc. B* **278**, 2098–2104. (doi:10.1098/rspb.2010.2293)
- Tamm S, Armstrong DP, Tooze ZJ. 1989 Display behavior of male calliope hummingbirds during the breeding season. *Condor* **91**, 272–279. (doi:10.2307/1368304)
- Boulenguez J, Berthier S, Leroy F. 2012 Multiple scaled disorder in the photonic structure of Morpho rhetenor butterfly. *Appl. Phys. A* **106**, 1005–1011. (doi:10.1007/s00339-011-6728-y)
- Durrer H, Villiger W. 1970 Schillerradien des goldkuckucks (*Chrysococcyx cupreus* (Shaw)) im elektronenmikroskop. *Cell Tissue Res.* **109**, 407–413.
- Clark Jr GA. 2004 Form and function: the external bird. In *Handbook of bird biology* (eds S Podulka, RW Rohrbach, R Bonney), pp. 3:1–3:70. Princeton, NJ: Princeton University Press.
- Lucas A, Stettenheim PR. 1972 Avian anatomy integument. *US Govern. Printing Office* **1**, 235–340.
- Durrer H. 1986 Colouration. In *Biology of the integument: vertebrates* (ed. J Bereiter-Hahn), pp. 239–247. Berlin, Germany: Springer.
- Zi J *et al.* 2003 Coloration strategies in peacock feathers. *Proc. Natl Acad. Sci. USA* **100**, 12 576–12 578. (doi:10.1073/pnas.2133313100)
- Prum RO, Torres RH, Williamson S, Dyck J. 1999 Two-dimensional Fourier analysis of the spongy medullary keratin of structurally coloured feather

- barbs. *Proc. R. Soc. Lond. B* **266**, 13–22. (doi:10.1098/rspb.1999.0598)
28. Kinoshita S. 2008 *Structural colors in the realm of nature*. Singapore: World Scientific.
 29. Joannopoulos JD, Johnson SG, Winn JN, Meade RD. 2008 *Photonic crystals: molding the flow of light (second edition)*, 2nd edn. Princeton, NJ: Princeton University Press.
 30. Newton I. 1704 *Opticks*. London, UK: Samuel Smith and Benjamin Walford.
 31. Land MF. 1972 The physics and biology of animal reflectors. *Progr. Biophys. Mol. Biol.* **24**, 75–106. (doi:10.1016/0079-6107(72)90004-1)
 32. Gardner A, Tchou C, Hawkins T, Debevec P. 2003 Linear light source reflectometry. *ACM Trans. Graph. (TOG)* **22**, 749–758. (doi:10.1145/882262.882342)
 33. Wang J, Zhao S, Tong X, Snyder J, Guo B. 2008 Modeling anisotropic surface reflectance with example-based microfacet synthesis. *ACM Trans. Graph. (TOG)* **27**, 41. (doi:10.1145/1360612.1360640)
 34. Westin S, Arvo J, Torrance KE. 1992 Predicting reflectance functions from complex surfaces. *ACM SIGGRAPH Comp. Graph.* **26**, 255–264. (doi:10.1145/142920.134075)
 35. Han C, Sun B, Ramamoorthi R, Grinspun E, Grinspun E. 2007 Frequency domain normal map filtering. *ACM Trans. Graph. (TOG)* **26**, 28:1–28:11. (doi:10.1145/1276377.1276412)
 36. Cook RL, Torrance KE. 1982 A reflectance model for computer graphics. *ACM Trans. Graph. (TOG)* **1**, 7–24. (doi:10.1145/357290.357293)
 37. Ward G. 1992 Measuring and modeling anisotropic reflection. *ACM SIGGRAPH Comp. Graph.* **26**, 265–272. (doi:10.1145/142920.134078)
 38. Poulin P, Fournier A. 1990 A model for anisotropic reflection. *ACM SIGGRAPH Comp. Graph.* **24**, 273–282. (doi:10.1145/97880.97909)
 39. Ashikmin M, Premože S, Shirley P. 2000 A microfacet-based BRDF generator. In *SIGGRAPH '00: Proc. 27th Annual Conference on Computer graphics and interactive techniques, July*, pp. 65–74. New York, NY: ACM Press/Addison-Wesley Publishing Co.
 40. Kajjya JT. 1985 Anisotropic reflection models. *ACM SIGGRAPH Comp. Graph.* **19**, 15–21. (doi:10.1145/325165.325167)
 41. Kajjya JT, Kay T. 1989 Rendering fur with three dimensional textures. *ACM SIGGRAPH Comp. Graph.* **23**, 271–280. (doi:10.1145/74334.74361)
 42. Marschner SR, Jensen HW, Cammarano M, Worley S, Hanrahan P. 2003 Light scattering from human hair fibers. *ACM Trans. Graph. (TOG)* **22**, 780–791. (doi:10.1145/882262.882345)
 43. Marschner SR, Westin S, Arbree A, Moon J. 2005 Measuring and modeling the appearance of finished wood. *ACM Trans. Graph. (TOG)* **24**, 727–734. (doi:10.1145/1073204.1073254)
 44. Zhao S, Jakob W, Marschner SR, Bala K. 2011 Building volumetric appearance models of fabric using micro CT imaging. *ACM Trans. Graph. (TOG)* **30**, 44:1–44:10. (doi:10.1145/2010324.1964939)
 45. Irawan P, Marschner SR. 2012 Specular reflection from woven cloth. *ACM Trans. Graph. (TOG)* **31**, 11:1–11:20. (doi:10.1145/2077341.2077352)
 46. Potton RJ. 2004 Reciprocity in optics. *Rep. Progr. Phys.* **67**, 717–754. (doi:10.1088/0034-4885/67/5/R03)
 47. Stokes GG. 1849 *On the Perfect Blackness of the Central Spot in Newton's Rings, and on the Verification of Fresnel's Formulas for the Intensities of Reflected and Refracted Rays*. Cambridge and Dublin Mathematical Journal **4**, 1–14.
 48. von Helmholtz H. 1896 *Handbuch der physiologischen Optik*. Hamburg, Germany: Verlag von Leopold Voss.
 49. Vukusic P, Stavenga DG. 2009 Physical methods for investigating structural colours in biological systems. *J. R. Soc. Interface* **6**, S133–S148. (doi:10.1098/rsif.2008.0386.focus)
 50. Stevens M, Párraga CA, Cuthill IC, Partridge JC, Troscianko TS. 2007 Using digital photography to study animal coloration. *Biol. J. Linnean Soc.* **90**, 211–237. (doi:10.1111/j.1095-8312.2007.00725.x)
 51. Dyck J. 1987 Structure and light reflection of green feathers of fruit doves (*Ptilinopus* spp.) and an Imperial Pigeon (*Ducula concinna*). *Biologische Skrifter* **30**, 2–43.
 52. Yoshioka S, Kinoshita S. 2002 Effect of macroscopic structure in iridescent color of the peacock feathers. *Forma* **17**, 169–181.
 53. Harvey JE, Vernold C. 1998 Description of diffraction grating behavior in direction cosine space. *Appl. Opt.* **37**, 8158–8160. (doi:10.1364/AO.37.008158)